Research Report

2003-22

Current stiff rectifiers with reverse blocking IGBTs and IGBTs with series diodes

F. Kieferndorf, M. Forster*, G. Venkataramanan & T.A. Lipo

University of Wisconsin-Madison
Dept. of Elec. and Comp. Engr..
1415 Engineering Dr.
Madison, WI 53706

* Dept. of Power electronics
Technical University of Ilmenau
98693 Ilmenau, Germany

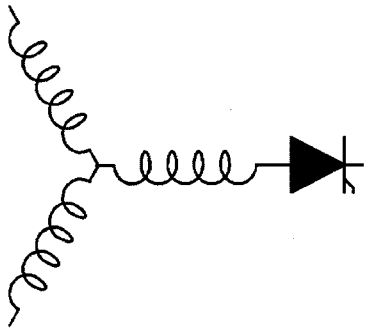

Wisconsin
Electric
Machines &
Power
Electronics
Consortium

University of Wisconsin-Madison
College of Engineering
Wisconsin Power Electronics Research Center
2559D Engineering Hall
1415 Engineering Drive
Madison WI 53706-1691

Current stiff rectifiers with reverse blocking IGBTs and IGBTs with series diodes

Frederick Kieferndorf Matthias Förster * Giri Venkataramanan, T.A. Lipo

University of Wisconsin-Madison
Dept. of Elec. and Comp. Eng.
1415 Engineering Dr.
Madison, WI 53706
(608)265-3821
kiefernd@ieee.org

* Dept. of Power Electronics
Technical University of Ilmenau
98693 Ilmenau, Germany

Keywords - discrete power devices, device applications, device characterization, efficiency, power semiconductor devices, semiconductor devices, three phase systems, user application experiences

Abstract - Current stiff converters (CSCs) have a well known requirement for reverse blocking type switching devices. This paper will discuss measurements of performance characteristics for a monolithic reverse blocking IGBT and an IGBT with a series diode. Measurement results and important characteristics will be presented and compared. Curve fit loss models will be applied to analyze the losses of each type of device in a current stiff rectifier (CSR) application. PCB designs for the two CSR realizations will be discussed in terms of the effect of the choice of device type on the size and parasitic inductances of the overall circuit. The characteristics of the devices in the CSRs will be compared to show how the PCB layout and devices interact. Finally a recommendation will be made as to which device is preferred for this application.

I. Introduction

In recent years, there has been increasing interest in ac-ac power converters employing a stiff current link as opposed to the more common stiff voltage link [1-5]. It is well known that current stiff converters (CSCs) require reverse blocking type switching devices for their realization. GTOs and thyristors have been commonly used for these applications at higher power levels. Although these devices are inherently reverse blocking, they have the disadvantage of complicated gate control and are suitable only for low frequency operation. It would be highly desirable to apply IGBTs in these applications due to their high frequency switching capability and simple voltage gate control. In practice this generally requires the use of a diode placed in series with the IGBT to provide the reverse blocking capability since IGBTs have generally been designed for use in voltage stiff converters where reverse blocking is not required. However, the additional device voltage drops in the forward conduction path results in a penalty of greater conduction losses. More recently, monolithic reverse blocking IGBTs have been introduced [6]. In principle, this would cut the silicon parts count in half and potentially reduce the total device losses. The reduction in the number of total parts could also have implications for the stray inductance in the circuit interconnections as well.

A comparative investigation has been conducted into the losses and switching behavior of bi-directional voltage blocking switch realizations: one a monolithic reverse blocking IGBT (RB-IGBT) and the second a combination of an IGBT with a series diode (IGBT-SD). They two switch types are than evaluated in terms of overall losses in a current stiff converter. A hardware setup was built to test both switch realizations under various voltage and current conditions to compile their switching characteristics. The characterization data was then used to evaluate their loss performance in a CSR. Furthermore, two printed circuit boards (PCBs) were designed to implement a CSR, one using the RB-IGBTs and the other using the standard IGBT-SDs. The hardware was then built to measure the characteristics of the rectifiers and to evaluate and compare the two topologies under real operating conditions. One key criterion is converter efficiency as this is one of the most common criticisms of a CSR compared to a voltage stiff rectifier.

In Section II, the characterization methods and results from the experimental investigations of the devices are presented. The realization of the CSR using the RB-IGBT and IGBT-SD devices are described in Section III. Power loss calculations in a CSR including conduction and switching losses based on the characterization data are presented in Section IV, which is followed by a brief concluding section.

II. IGBT Device Characterization

Commercial versions of the RB-IGBT are relatively new on the semiconductor market [6-8]. The number of discrete device packages or dies in a packaged module for current stiff converters (CSCs) can potentially be reduced from twelve to six using the new reverse blocking switches, resulting in reduced size and cost of the rectifier/inverter. The devices used in these experiments are from IXYS.

Since the availability of detailed performance data for these devices are limited, measurements were made to develop relationships for switching and conduction losses under typical operating conditions. The ratings of the devices tested are shown in Table I. Although the standard IGBT used for the IGBT-SD composite device testing had a rated current of 48A, an Ultra-Low V_{CE} IGBT with a 60A rated current was used in the realization of the rectifier. The 48A device will provide larger values for the switching losses since it is a HiPerFast type IGBT. The series diode is a HiPerFRED epitaxial diode with soft recovery.

Table I - Key parameters for devices used in testing

	Standard low V_{CE} IGBT	Diode	Standard fast IGBT	RB-IGBT
	IXGH31N60	DSEP60-06A	IXGH24N60B	IXRH50N60
V_{fblock}	600 V	0 V	600 V	600 V
V_{rblock}	0 V	600 V	0 V	600 V
I_{rated}	60 A	60 A	48 A	60 A

A boost power converter arrangement was chosen as the test circuit to allow observation of the forward and reverse bias switching and operating characteristics simultaneously. The circuit diagram with the voltage and current reference designations is shown in Figure 1. The duty cycle of the main switch was held at 15% (lower limit of the function generator used to create the switching signals) to produce input and output voltages that were nearly identical. Each throw of the single pole double throw switch in the boost converter was either a RB-IGBT or an IGBT-SD. In the forward biased (FB) throw the forward characteristic could be measured and in the reverse biased (RB) throw the reverse blocking behavior could be observed. The reverse recovery behavior of the RB-IGBT compared to the IGBT-SD was of particular interest in these experiments.

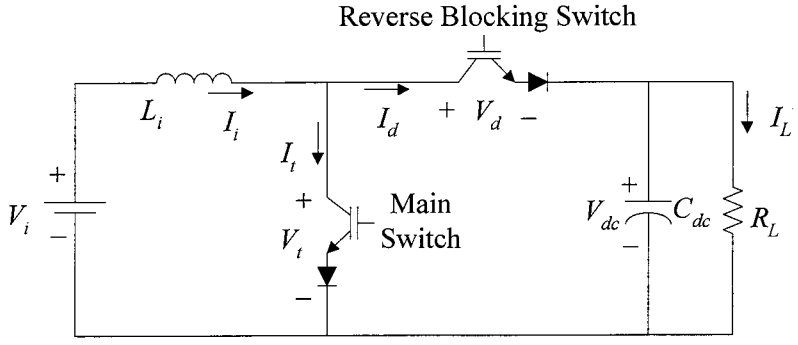

Figure 1 - Boost converter test circuit for measuring both forward and reverse blocking behavior of devices.

The reverse recovery behavior during turn-on and the voltage overshoot during turn-off for both types of switches were observed in the experiments. The reverse recovery current is generated in the RB throw when the FB throw is turned on. A negative voltage is then applied across the RB throw turning it off. Because the reverse recovery current is reflected in the FB throw over and above the inductor current I_i, it causes high losses in the FB switch during turn-on. The resulting reverse recovery peak current for the RB-IGBT was over three times higher than for the IGBT-SD. Often the rated current maximum was reached at low forward current for the RB-IGBT because of this. However the voltage overshoot for the IGBT-SD was two times higher than for the RB-IGBT. These issues will be further discussed in the following section describing the operation of the CSR.

The switching behavior for turn-on and turn-off with V_i of 100V, 200V and 300V was observed over a range of currents. An attempt was made to adjust the current in steps from 1A up to 30A for each voltage level. The main limiting factor was the reverse recovery current from the RB throw flowing through the FB throw. Several RB-IGBT devices were destroyed when the combination of switching frequency and peak current exceeded the thermal capacity of the device, thus the maximum non-destructive value attained for I_i was 10A. The current and voltage in the FB throw and in the RB throw for these three voltages levels were captured for use in numerical calculations to determine the turn-on and turn-off losses. The same measurements were done for both the IGBT-SD and RB-IGBT. Switching waveforms are shown in Figures 2(a) and 2(b). The extremely large reverse recovery current in the RB-IGBTs is readily evident in the figures. In both cases the forward current is about 15A. For the IGBT-SD the peak reverse recovery current is about 15A but for the RB-IGBT the peak reverse recovery current is about 50A.

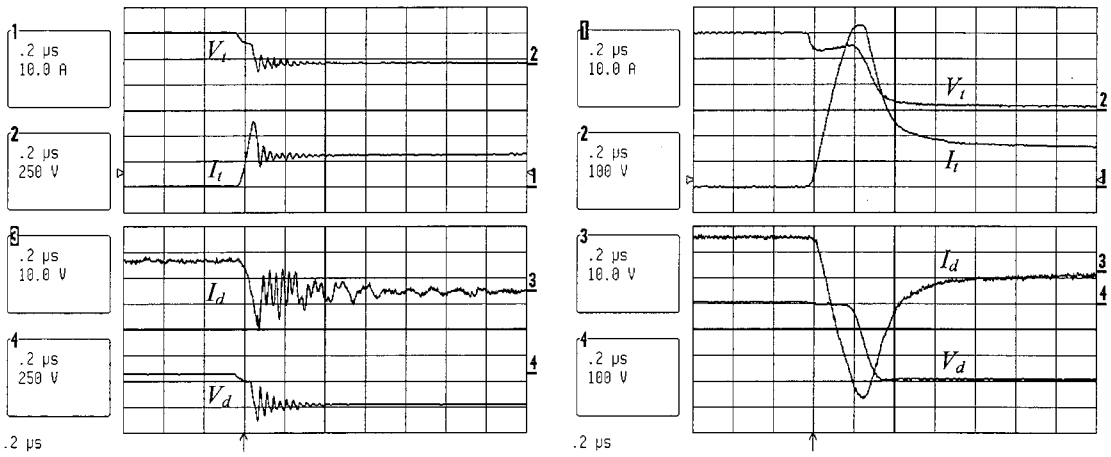

(a) (b)

Figure 2 - Waveforms of (a) IGBT-SD and (b) RB-IGBT: I_t - Main switch current, V_t - Main switch voltage, I_d - Reverse switch current, V_d - Reverse switch voltage.

The voltage and current waveforms were recorded into a data file and the switching losses were calculated using Matlab®. The energy was calculated as the following:

$$E = \int I_c \, V_{ca} \, dt \tag{1}$$

where I_c is the device collector current and V_{ca} is the voltage from the IGBT collector to the diode anode of one throw. For each calculation one voltage and one current waveform containing both a turn-on event and a turn-off event were used. The turn-on start time was determined as the instant that the on-state voltage began to rise. The turn-on end time for the RB-IGBT was located by finding the local minimum in the current just after the reverse recovery current peak. The turn-on end time for the IGBT-SD was located by finding the first zero crossing of the voltage just after the reverse recovery current peak. The turn-off start time was determined as the instant that the initial voltage

began to fall. The turn-off end time for both devices was located by finding the time when the current fell below 1% of the on-state current.

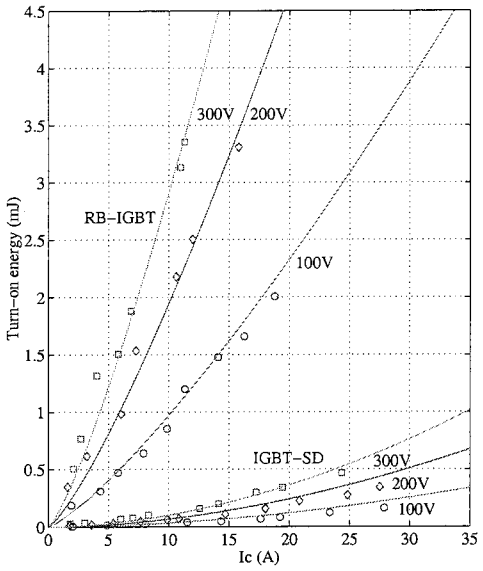

Figure 3 - Calculated turn-on energy vs. collector current for RB-IGBT(upper) and IGBT-SD (lower) for different voltages.

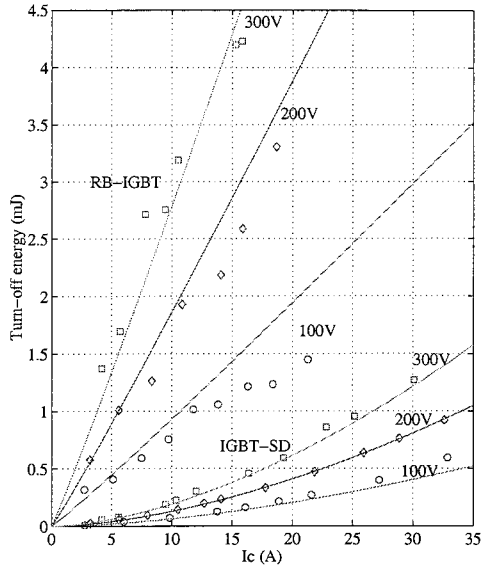

Figure 4 - Calculated turn-off energy vs. collector current for RB-IGBT(upper) and IGBT-SD (lower) for different voltages

Figure 3 shows the turn-on energy and Figure 4 shows the turn-off energy for both IGBT types at the measured voltage and current levels. The equations used to fit the measured data [9] for both turn-on and turn-off have the general form:

$$E_{loss} = k\, I_c^m \frac{|V|}{V_{sp}} \quad \text{(J)} \tag{2}$$

where k and m are curve fitting constants, V_{sp} is the off-state commutation voltage present during the data measurement. The switching energy is then a function both of the instantaneous off-state voltage (V) and on-state collector current (I_c). It can be seen that the RB-IGBT has much larger switching losses than the IGBT-SD.

The forward characteristic for both switch types was determined by operating the CSR boards with a resistive load. The 60A, low V_{CE} devices were used in the IGBT-SD rectifier. The forward voltage as a function of forward current equation used to fit the measured data is the following:

$$v_{fwd} = v_o + r_o\, I_c^m \quad \text{(V)} \tag{3}$$

where v_o, r_o and m are fitting constants. The forward voltage is v_{fwd} and the on-state current is I_c. The measured data points overlaying the curve from (3) are shown in Figure 5. Figure 6 shows a plot of conduction losses calculated at each data point as function of the forward current compared to the product of on-state voltage and current from the curve fit equations. Clearly, the RB-IGBT conduction losses are significantly smaller than those of the IGBT-SD.

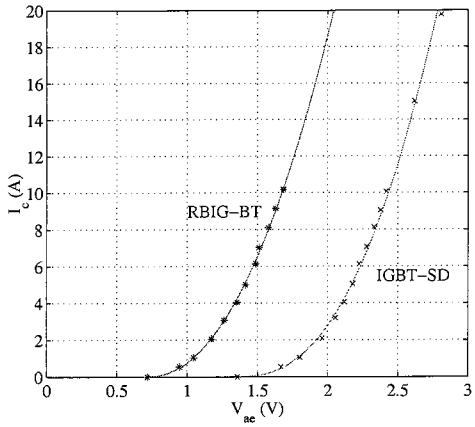

Figure 5 - Experimental (*,x) forward I-V characteristics compared with fitted curves(—, ····) for RB-IGBT and IGBT-SD.

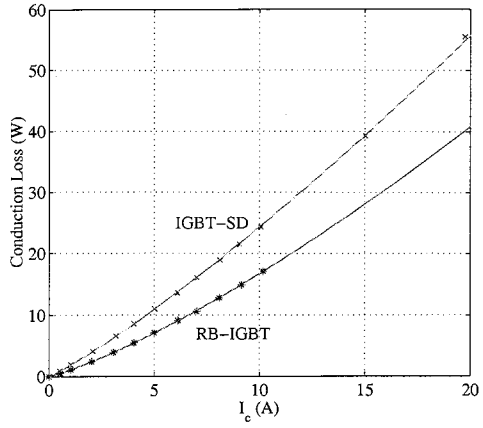

Figure 6 - Conduction losses vs. forward current: experimental data (*,x) compared to product of v_{fwd} (3) and I_c. (—, ····).

III. Device behavior in the CSR PCB

In addition to the experimental characterization of these devices, a CSR prototype using a printed circuit board was constructed to study their performance in an application. The power circuit diagram of the CSR is shown in Figure 7 for reference. The PCB-based rectifiers were designed to operate with a rated continuous current of 30A. The traces were made with 1oz copper (0.034mm thickness). The components of the three phases were laid out symmetrically using the smallest footprint for the power circuit to produce equal length commutation paths with reduced stray inductance and to distribute the switching stresses equally among the devices.

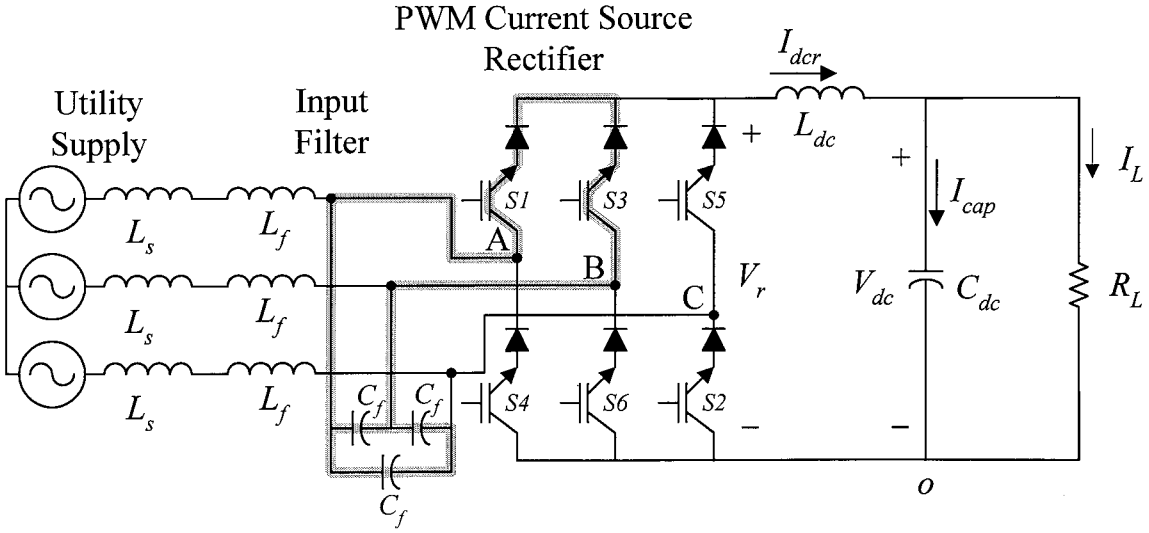

Figure 7 - CSR PCB circuit diagram where the IGBT/diode pairs are either IGBT-DS or RB-IGBT. An example commutation path from S1 to S3 is shown in color.

The traces were designed to avoid overheating because of the relatively high current on the board. Standard PCB design graph curves from ANSI/IPC-D-275 were used to analyze the performance of the board layout [10]. Trace temperature rise can be determined given the rated current, copper weight and trace width. For a current of 30A and a temperature rise of 75°C the trace width should be

about 10.2mm (0.4in). The minimum temperature rise shown for 30A would be 45°C corresponding to an interpolated trace width of 13.3mm (0.525in). The minimum trace width on the completed PCBs is about 15mm, which was found to keep the temperature rise quite low.

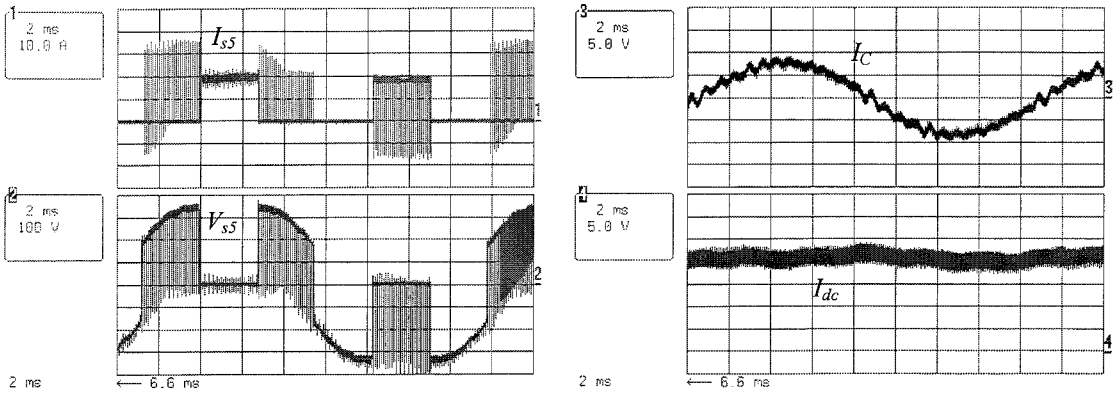

(a) (b)

Figure 8 - Operating waveforms from the IGBT-SD CSR showing a fundamental period: (a) device waveforms from the *upper* switch of leg C, (b) phase C input current and DC link current.

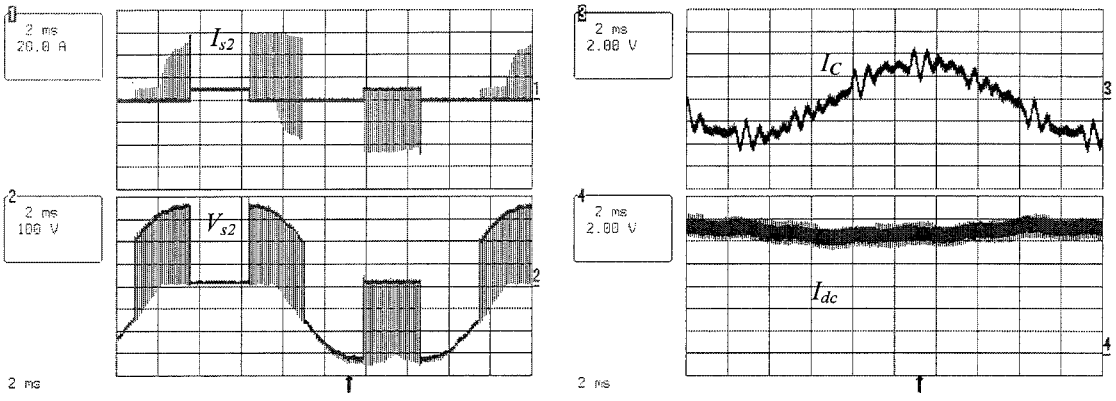

(a) (b)

Figure 9 - Operating waveforms from the IGBT-RB CSR showing a fundamental period: (a) device waveforms from the *lower* switch of leg C, (b) phase C input current and DC link current.

Both types of CSRs were operated with full supply voltage (line-line input rms voltage of 230V) and a constant resistive load. The modulation index was adjusted to change the DC bus voltage and determine the load current. The CSR with RB-IGBTs could only be loaded up to 10A as mentioned previously. The other CSR board could be safely operated up to the full load current of 30A because the peak current was only 50% higher than the forward current (~45A) and reverse recovery time is relatively small.

Some example waveforms are shown in Figures 8 and 9. The voltage and current reference directions for the devices are in the same sense as in Figure 1 (from IGBT collector to diode anode). It is important to note that the scales on the current waveforms of the two CSR board types are different. The RB-IGBT load current is 10A and device current (in this case the lower phase C leg) is seen to have very high reverse recovery currents up to the device maximum of 60A. It should also be noted that the RB-IGBT voltage waveform is much smoother looking than the IGBT-SD due to the difference in voltage overshoot. The phase C supply current is also nearly 180° out of phase for the two boards because measurements were made in the upper leg (S5) for the IGBT-SD and the lower leg (S2) for the RB-IGBT.

One of the critical issues in the design of a CSR is the stray inductance in the switching path between devices on the upper dc rails (i.e. between any two of S1, S3 or S5) or the lower dc rails (i.e. between any two of S4, S6 or S2). An example commutation path between S1 and S3 is shown in green in Figure 7. The high di/dt of the devices during switching can interact with the stray inductance to cause damaging overvoltages. Input filter capacitors and snubber capacitors are connected from line to line on the three phase input to provide a low impedance path for the switching current transient. Filter inductors placed in series with the input capacitors form a low pass filter to reduce the harmonic current injection into the utility supply as well. From the figure the total expected capacitance in the commutation path is $3/2C_f$.

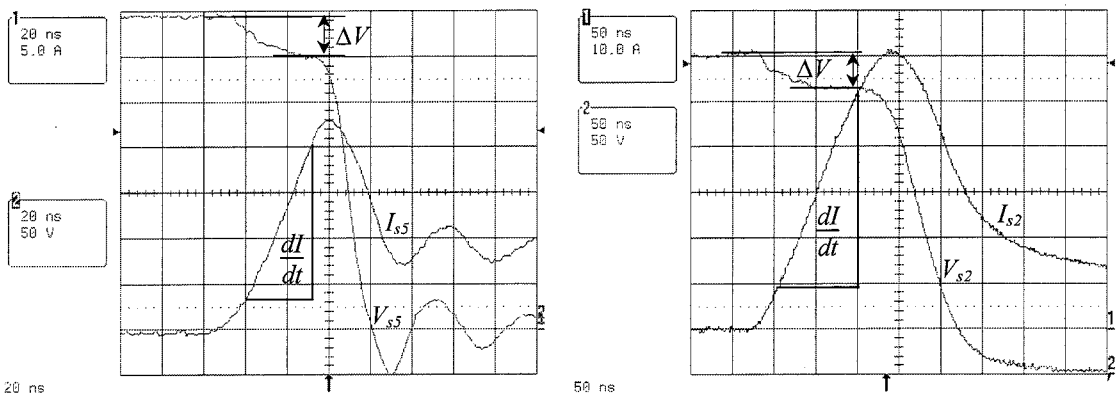

(a) (b)

Figure 10 - Waveforms from CSR with (a) IGBT-SDs and (b) RB-IGBTs showing the voltage dip due to the stray inductance during turn-on.

The stray inductance in the circuit can be estimated by looking at the voltage dip during the device turn-on. At this point the device that is turning off is not yet blocking any voltage so the voltage dip is due solely to the stray inductance. The waveforms for the two device types are shown in Figure 10 (a) and (b) indicating the necessary measurements. The inductance value can be calculated with the following equation from [11]:

$$L_\sigma = \frac{\Delta V}{dI/dt} \text{ (H)} \tag{4}$$

The average inductance values from the data measured over a range of load current values were determined to be 79nH for the IGBT-SD and 86nH for the RB-IGBT.

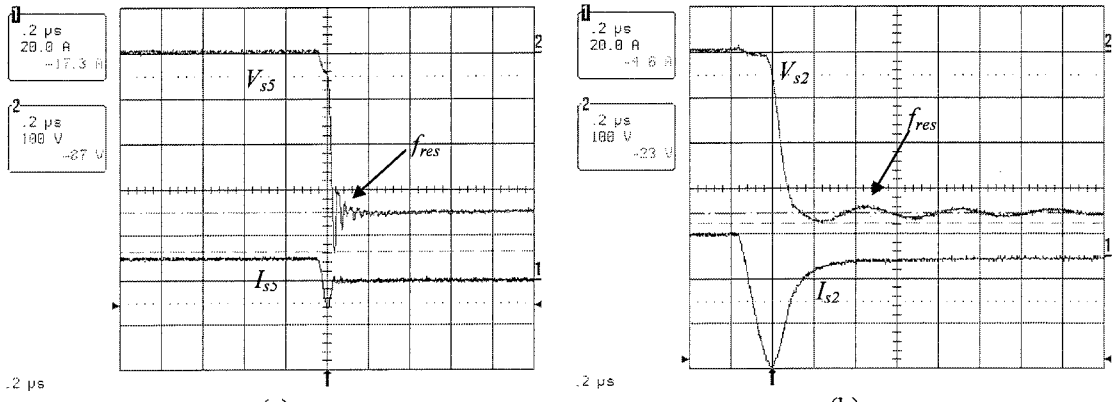

(a) (b)

Figure 11 - Waveforms from CSR with (a) IGBT-SDs and (b) RB-IGBTs showing reverse recovery and voltage overshoot during turn-off.

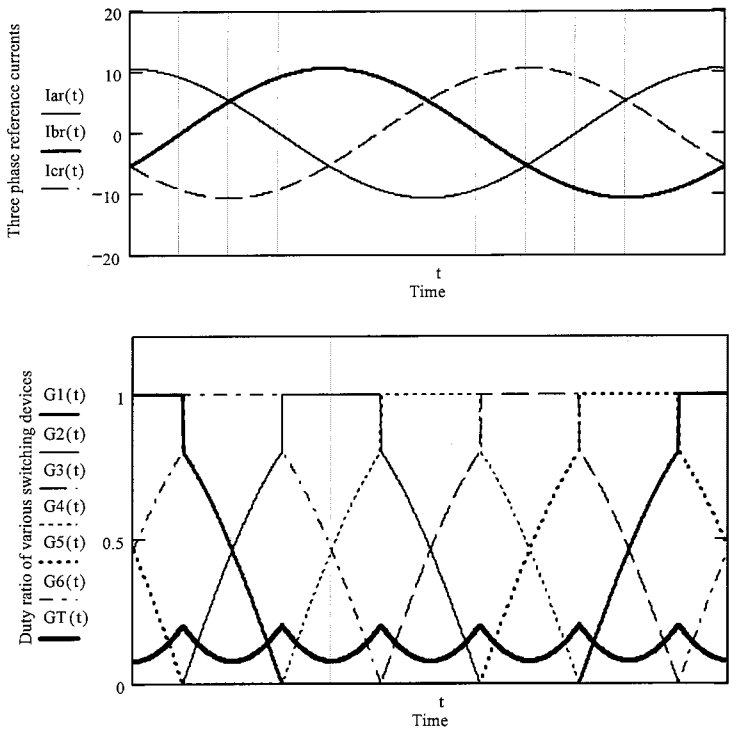

Figure 12 - Illustration of three phase current reference waveforms and duty ratio of various switch throws of the PWM current source rectifier.

The effective capacitance seen during the switching transient can be determined from the resonant frequency seen in the voltage waveform after each turn-off. This resonance is indicated for the two device types in Figure 11 (a) and (b). The RB-IGBT circuit exhibits a resonant frequency of 2.2MHz and the IGBT-SD circuit has a resonance at about 17MHz. The resulting capacitance from these measured resonant frequencies and the stray inductance calculated earlier comes to 570pF for the RB-IGBT and 11pF for the IGBT-SD. There is no simple way to correlate these values with the physical capacitors installed on the boards (equal in both cases) or the internal device capacitances. One feature that is apparent in Figure 11 is the difference in the reverse recovery snap-off of the two switch types which may be exciting different resonances. The device capacitances are also significantly different (RB-IGBT ~ 3x larger than IGBT-SD), which when coupled with the frequency dependence of the PCB impedances may be causing the unexpected results. The circuit geometry causes very complex frequency dependent behavior [12]. The source of the effective impedance is a subject of further research.

The maximum voltage overshoot during commutation is also visible in Figure 11. The overvoltage during turn-off in the CSR with RB-IGBTs is negligible. For the CSR with the IGBT-SDs, the overvoltage was about 14.5% of the rated device voltage (87V) as shown in Figure 11(a), which is also quite good. Since the main concern with the stray inductance is the resulting overvoltage due to the switch di/dt during commutation these results indicate that the values achieved are well within the device ratings in both cases.

IV. CSR Power Loss

The three phase reference current waveforms and the corresponding duty ratio of various switching devices of the three phase rectifier bridge used for unity power factor rectification are illustrated in Figure 12. The illustrations are at a dc current of 12A, input line-line rms voltage of 230V and a power throughput of 3kW. In Figure 12, GT corresponds to the zero state duty ratio, while other

waveforms correspond to the various throws of the CSR. The modulation strategy used for the converter is similar to that used in [13]. At a given instant of time, one of the IGBTs is always clamped and the two other IGBTs are switched alternately.

Conduction losses in the converter are a function of the forward voltage drop of the device and the current flowing through the device. At any instant of time, the dc link current flows through one of the top throws of the three phase rectifier bridge and through one of the bottom throws of the three phase rectifier bridge. Hence the total conduction losses may be estimated using the curve fit expression of conduction losses as

$$P_{cn} = 2\, I_{dc}\,(v_o + r_o\ I_{dc}^{mc}) \tag{5}$$

where r_o, m_c and v_o are curve fit parameters for the device as illustrated in Figures 4 and 5.

Due to the three phase symmetry of the modulation process, the total converter switching losses repeat periodically at six times the fundamental frequency of the input voltage waveform. Hence the average switching losses can be computed over a 60° interval and averaged as

$$P_{sw}(F_s) = F_s\left[\frac{k_{on} I_{dc}^{mon}}{V_{spon}} + \frac{k_{off}\, I_{dc}^{moff}}{V_{spoff}}\right]\frac{9V_{pk}}{\pi} \tag{6}$$

where k_{on}, k_{off}, m_{on}, m_{off}, V_{spoff} and V_{spon} are curve fit parameters for the device as illustrated in Figures 6 and 7 and V_{pk} is the phase to neutral peak voltage.

Using the above equations, total power converter losses for a CSR can be determined as a function of the switching frequency as illustrated in Figure 13. It may be noticed from the figure that due to the high switching loss penalty of reverse blocking IGBTs and the high conduction loss penalty of IGBTs with series diodes, make each of them preferable for low switching frequency and high switching frequency applications, respectively.

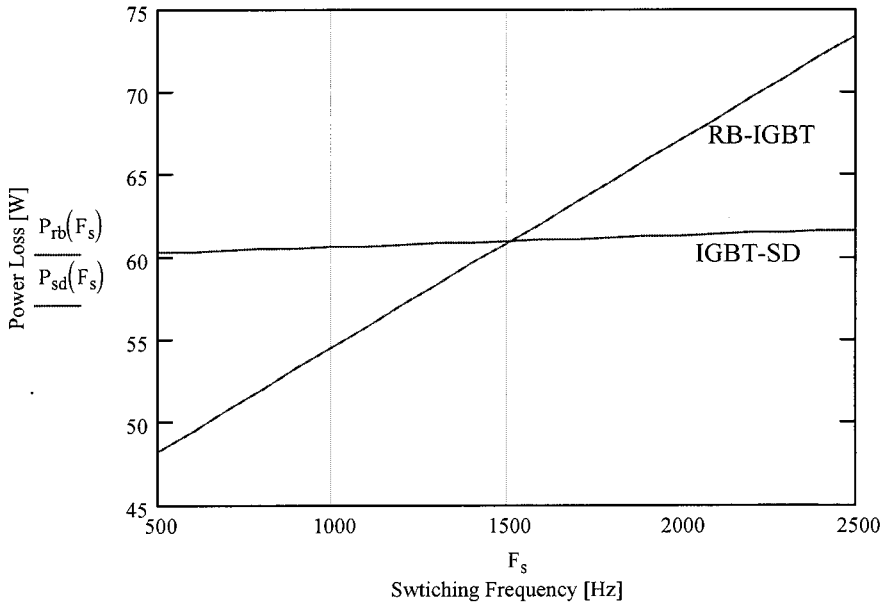

Figure 13 - Total losses as a function switching frequency for RB-IGBT (—) and IGBT-SD (—) with I_{dc} = 12A and input line - line voltage of 230Vrms.

V. Conclusion

This paper has presented the results from a detailed experimental characterization of reverse blocking IGBTs that may be used in current stiff converters. Monolithic and discrete realizations were studied in the characterization process. Results of the investigations point out that although the monolithic devices have vastly superior conduction properties, they suffer from unduly large reverse recovery losses during switching. Use of a RB-IGBT would require a large current derating of the device in order to realize switching frequencies upwards of a few kHz. Using state of the art devices, the break-even frequency where the reduced conduction losses of the RB-IGBT are an advantage over the IGBT-SD occurs at a switching frequency of 1.5kHz in a typical application. However, if the reverse recovery characteristics of these devices could be improved they could result in significant advantages in current stiff converters. Thus the conclusion for the current state of the art is that the discrete realization is preferred for the CSR application discussed due to the much smaller overall losses at the rated switching frequency of 10kHz.

Acknowledgment

The authors would like to thank the Wisconsin Electric Machines and Power Electronics Consortium (WEMPEC) for their support of the research presented in this paper.

References

[1] I. Wallace, A. Bendre, J.P. Nord, G. Venkataramanan, "A unity-power-factor three-phase PWM SCR rectifier for high-power applications in the metal industry," IEEE Transactions on Industry Applications, vol. 38, pp. 898- 908, July/August 2001.

[2] V. Nedic, *Low-cost current-fed PMSM drive system with sinusoidal input current.* PhD thesis, University of Wisconsin-Madison, 2002.

[3] H. F. Bilgin, K. N. Kose, G. Zenginobuz, M. Ermis, E. N. I. Cadirci, and H. Kose, "A unity-power-factor buck-type PWM rectifier for medium/high-power DC motor drive applications," IEEE Transactions on Industry Applications, vol. 38, pp. 1412-1425, September/October 2002.

[4] A. Bendre, I. Wallace, J.P. Nord, G. Venkataramanan, "A current source PWM inverter with actively commutated SCRs", IEEE Transactions on Power Electronics, vol. 17, pp. 461-468, July 2002.

[5] F. D. Kieferndorf, M. Förster, and T. A. Lipo, "Reduction of DC Bus Capacitor Ripple Current with PAM/PWM Converter," in Conference Record of the Industry Applications Society Annual Meeting (IAS), vol. 4, pp. 2371-2377, 2002.

[6] A. Lindemann, "A new IGBT with reverse blocking capability," in European Conference on Power Electronics and Applications (EPE), pp. 1-7, 2001.

[7] S. Bernet, T. Reimann, T. Taleb, and J. Petzoldt, "Special effects of IGBTs in ZCS and ZVS applications," in Proceedings of PCIM, Nurnberg, pp. 203-217, 1994.

[8] S. Huth and S. Winternheimer, "The switching behaviour of an IGBT in zero current switch mode," in European Conference on Power Electronics and Applications (EPE), pp. 312-316, 1993.

[9] T. Matsuo, S. Bernet, R. S. Colby, and T. A. Lipo, "Modeling and simulation of matrix converter/induction motor drive," Mathematics and Computers in Simulation, vol. 46, pp. 175-195, 1998.

[10] ANSI/IPC-D-275, "Design Standard for Rigid Printed Boards and Rigid Printed Board Assemblies", Figure 3-4, Page 10, IPC, September, 1991.

[11] "Measurement of the circuit stray inductance L_σ", eupec - Application Note.

[12] W. Teulings, J.L. Schanen and J. Roudet, "MOSFET switching behaviour under influence of PCB stray inductance", in Conference Record of the Industry Applications Society Annual Meeting (IAS), vol. 3, pp. 1449-1453, 1996.

[13] L. Malesani and P. Tenti, "Three-phase AC/DC PWM converter with sinusoidal AC currents and minimum filter requirements," IEEE Transactions on Industry Applications, vol. IA-23, pp. 71-77, 1987.